



Article

Drought Risk Assessment and Monitoring of Ilocos Norte Province in the Philippines Using Satellite Remote Sensing and Meteorological Data

Christian Albert Alonzo¹, Joanna Mae Galabay¹, Margadrew Nicole Macatangay¹, Mark Brianne Magpayo¹ and Ryan Ramirez^{1,2,*} 

¹ Department of Civil Engineering, University of Santo Tomas, Manila 1008, Philippines

² Division of Earth and Space Sciences, National Research Council of the Philippines, Taguig 1631, Philippines

* Correspondence: raramirez@ust.edu.ph

Abstract: Drought has been known to be a natural hazard reflecting geographic and climatic characteristics. Satellite technology advancements have benefited drought assessment and monitoring to formulate plans for dealing with this slow-onset disaster. However, combining satellite remote sensing (RS) and meteorological data for drought monitoring is lacking in the literature. This study uses satellite RS and meteorological-based drought indicators to assess drought risk in the Ilocos Norte, Philippines. Data analysis included the retrieval of vegetation conditions using Sentinel-1 and Sentinel-2 data. The standardized precipitation index (SPI) and Keetch–Byram drought index (KBDI) were calculated to account for climatic variabilities. Results revealed that the Sentinel-1 backscatter coefficient decreased by -2 dB in the cropland area, indicating crop growth irregularities compared to grassland areas. These irregularities were supported by Sentinel-2 normalized difference vegetation index (NDVI) strong fluctuations during the two-year observation period. A significant coefficient of determination ($R^2 > 0.60$) between the Sentinel-1 backscatter coefficient and Sentinel-2 NDVI was observed for the study area. On the one hand, only KBDI significantly correlated ($R^2 > 0.60$) with the cropland area's RS data-derived drought indicators. These results revealed RS data variability for drought risk management but are still valuable for developing an early warning system.

Keywords: drought; remote sensing; Sentinel-1 SAR data; Sentinel-2 optical data; Ilocos Norte



Citation: Alonzo, C.A.; Galabay, J.M.; Macatangay, M.N.; Magpayo, M.B.; Ramirez, R. Drought Risk Assessment and Monitoring of Ilocos Norte Province in the Philippines Using Satellite Remote Sensing and Meteorological Data. *AgriEngineering* **2023**, *5*, 720–739. <https://doi.org/10.3390/agriengineering5020045>

Academic Editor: Murali Krishna Gumma

Received: 22 February 2023

Revised: 6 April 2023

Accepted: 11 April 2023

Published: 13 April 2023



Copyright: © 2023 by the authors. Licensee MDPI, Basel, Switzerland. This article is an open access article distributed under the terms and conditions of the Creative Commons Attribution (CC BY) license (<https://creativecommons.org/licenses/by/4.0/>).

1. Introduction

Drought is a natural hazard that reflects the region's exposure to various geographic and climatic characteristics. Due to its widespread impacts over a large area in a certain period, it is considered more potent than other natural disasters, especially in areas that heavily rely on agricultural-based occupations [1]. Mainly attributed to low precipitation for an extended period, drought provides negative implications regarding economic and social functions. The consequences of such drought-related outcomes have severely inhibited the proper functioning of the community regarding water supply, productivity, and food security [2]. Hence, the evaluation of probable drought-risk areas must be addressed and mitigated through data-based assessments.

Drought indicators represent data to quantify or measure drought severity in a particular area. It uses information on rainfall, streamflow, soil moisture, and other hydro-meteorological evidence to monitor vegetation conditions. With this, various indices can be used to establish the amount of precipitation for a certain period and accordingly compare its deviation from established standards. Some of the widely used meteorological-based indices include the standardized precipitation index (SPI) [3–8], standardized precipitation index and evapotranspiration index (SPEI) [3,5–7,9,10], multivariate standardized precipitation index (MSPI) [11,12], rainfall anomaly index (RAI) [13,14], and Palmer drought severity index (PDSI) [8,15,16]. However, the scarcity and high spatiotemporal variability of

meteorological stations across different regions limit the successful utilization of these meteorological-based indices for drought assessment and monitoring [17].

The application of remote sensing (RS) in drought studies lies in its capability to observe changes in a geographic environment [18]. It can monitor a particular area's condition before, during, and after a disaster strikes. Similarly, a geographic information system (GIS) creates a centralized mechanism for the RS data through mapping and spatial analysis for a particular disaster scope. Likewise, advancements in satellite technology have been beneficial in drought assessment and monitoring, which help formulate plans to deal with this slow-onset disaster [19,20]. Satellite observations have provided significantly contributed to accurately visualizing surface parameters in the possible occurrence and severity of drought for a certain period [21–24]. Specifically, Sentinel-2 and Landsat optical satellite-derived indices are widely used to evaluate drought on a regional scale [25–33]. The most commonly used optical RS data-derived drought indicators include the normalized difference vegetation index (NDVI), normalized difference water index (NDWI), vegetation condition index (VCI), and enhanced vegetation index (EVI). However, optical satellite data are highly affected by unpredicted atmospheric conditions (i.e., cloud contamination), limiting the collection and utilization of quality optical satellite imagery despite being acquired at shorter time windows with zero costs.

On the other hand, synthetic aperture radar (SAR) data complement optical satellite data in regions with considerable cloud cover density in investigating drought. SAR is an active radar imaging technology that works in all weather conditions, day and night. For example, the fleet of twin Sentinel-1 satellites has provided free accessible archived medium-resolution SAR data, which the scientific community utilizes for various earth observation and geohazard applications such as floods [34,35], volcano eruptions [36,37], earthquakes [38,39], landslides [40–42], and land subsidence [43–45]. However, limited studies have utilized Sentinel-1 SAR data for drought analysis [46–48]. Specifically combining freely available optical satellite data (i.e., Sentinel-2 and Landsat-8) and space-borne SAR data (i.e., Sentinel-1) for drought monitoring is rarely reported in the literature [49–51]. Statistical analysis proving the relationship among drought indicators derived across RS and hydrological data is also lacking in the literature.

Amid all the innovations and advancements of RS and GIS technologies occurring worldwide, the Philippines is still evidently lacking. Despite the frequent severe weather and climatic events that affect the country each year, mitigation and improvement of conditions are challenging to achieve even up to now because of the scarcity of available and freely accessible data and research in the Philippines. Specifically, the Philippines' monitoring drought system is weak, resulting in multiple adverse drought impacts and emergency events. The World Health Organization (WHO) Collaborating Centre for Research on the Epidemiology of Disasters (CRED) recorded eight droughts that occurred in the country affecting 6.5 million people and causing 64.4 million dollars in damage to livelihoods and properties [52]. This record emphasizes the need for the country to improve its technologies concerning the analysis of weather events aside from the numerous typhoons entering the country each year. Mainly, the Ilocos Norte Region in the Philippines has been one of the worst-hit areas as more than 2000 ha of high-value crops, such as rice and corn, were reported to be dried out and destroyed due to water shortage and warmer temperatures, as well as the intensifying El Niño conditions [53]. Damages to livestock and the environment have also been evident as a significant population in Ilocos Norte depends on the agricultural industry.

This study's overall objective is to promote the application of RS data in the Philippines' drought risk management plan. Specifically, the study assesses Sentinel-1's backscatter coefficient and Sentinel-2's NDVI for drought investigation. The study also aims to quantitatively test the correlations between satellite and meteorological data-derived indices through statistical analysis. Lastly, the study aims to provide a drought early warning system (EWS) using different drought indicators.

2. Study Area

Ilocos Norte Province is located in the northwest part of the Philippines and geographically between N 17°48' and N 18°29' latitude and E 120°58' and E 120°58' longitude (Figure 1). The province has a total land area of 362,291 ha, more than 33% of which is dedicated to agriculture and forestry [54]. Ilocos Norte is a central crop-producing area in the Philippines, allowing the region to be a key area for rice production and a significant rice supplier [55].

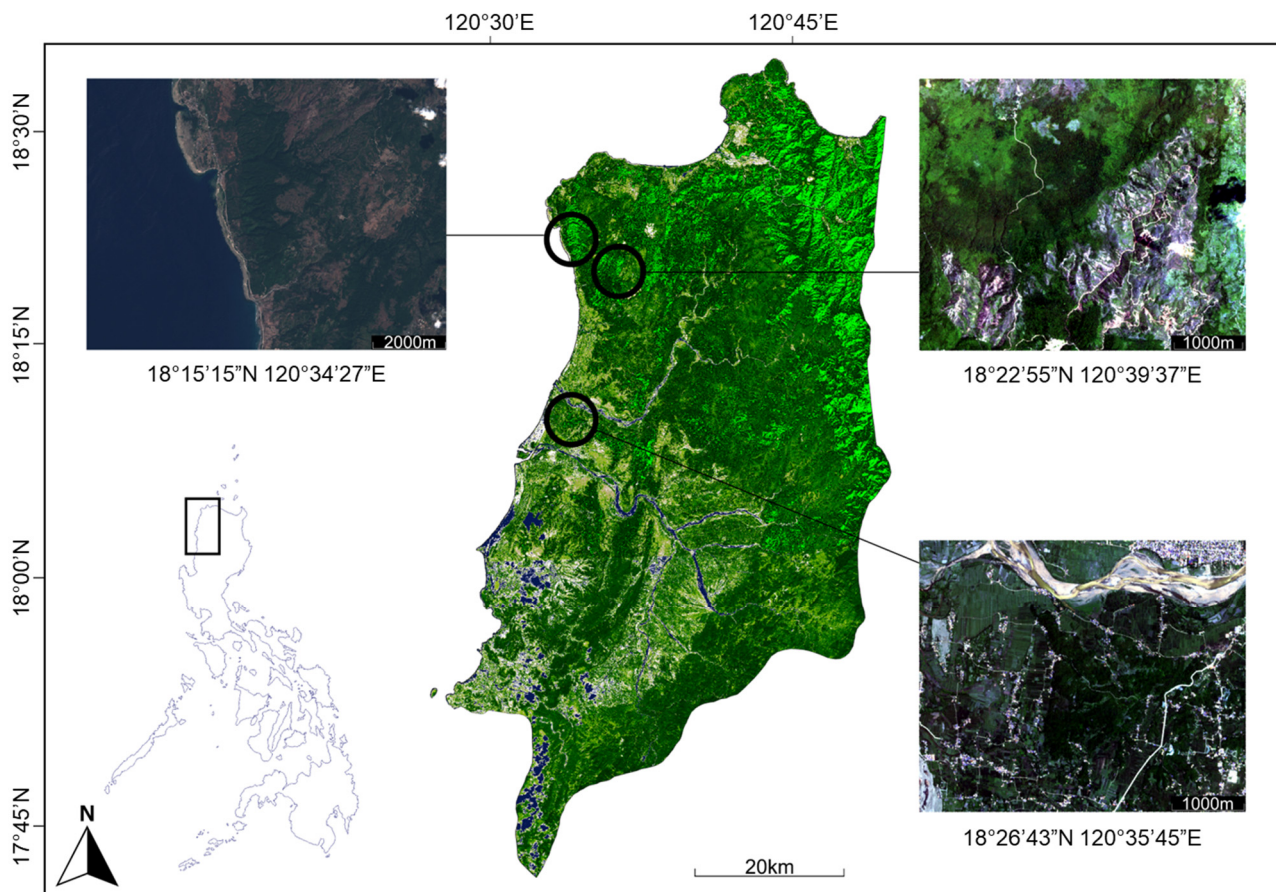


Figure 1. The map shows the regional boundary of the Ilocos Norte region in the Philippines and the cloud-free Sentinel-2 optical images of the cropland and grassland areas investigated in the study.

For this study, data gathering was focused on Ilocos Norte's capital, Laoag City. The city is located in the west-central part of the province. According to the Philippine Atmospheric, Geophysical and Astronomical Services Administration (PAGASA), the temperature in Laoag can go as high as 41.8 °C during the dry season and as low as 11 °C during the rainy season (PAGASA, 2018). The majority of croplands in Ilocos Norte are rainfall-dependent or in rained conditions. The climate experienced in the province is classified as Type I, which is indicated by a distinct dry and wet season. During the wet season, from May to October, the rice-farming activity highly depends on rainfall.

On the other hand, farmers use groundwater for supplemental irrigation during the dry season, which happens from November to April [56]. The average annual rainfall of Ilocos Norte is 2000 mm, and more than 90% of it happens during the wet season. However, the province has been experiencing way below average rainfall, resulting in damaged crops in recent years [57].

3. Materials and Methods

In this study, drought assessment was performed based on remote sensing data and meteorological data. The remote sensing data derived from Sentinel-1 and Sentinel-2 satellite missions were used to identify vegetation conditions. SPI and the Keetch–Byram drought index (KBDI) were calculated from precipitation and temperature to account for climatic variabilities in the region.

3.1. Sentinel-1 SAR Data

Sentinel-1 conveys a single C-band wavelength operating at a center frequency of 5.405 GHz. It comprises two satellites, Sentinel-1A and Sentinel-1B, launched in April 2014 and April 2016, respectively. Equipped with SAR, these satellites can operate at wavelengths not impeded by cloud cover or illumination, allowing data acquisition under any time and weather conditions. The 12-day repeat orbit cycle of each Sentinel-1 satellite and ancillary orbital baselines permit SAR data to provide coherent change detection applications useful for assessing land surface conditions.

Sentinel-1 SAR data were retrieved from the European Space Agency (ESA) via the Alaska Satellite Facility (ASF) database. The C-band Sentinel-1 analysis was carried out using 24 monthly scenes between 1 January 2019, and 31 December 2020, covering the dry and wet seasons from 2019 to 2020 (Table 1). Each scene contained two layers of the backscattering coefficient, σ° , in vertical–vertical (VV) and vertical–horizontal (VH) polarizations which were converted into decibels units (dB).

Table 1. Sentinel-1 synthetic aperture radar (SAR) dataset used in the study.

No.	Acquisition Date	Pass	No.	Acquisition Date	Pass
1	28 January 2019	Ascending	13	23 January 2020	Ascending
2	21 February 2019	Ascending	14	28 February 2020	Ascending
3	17 March 2019	Ascending	15	23 March 2020	Ascending
4	27 April 2019	Ascending	16	28 April 2020	Ascending
5	28 May 2019	Ascending	17	22 May 2020	Ascending
6	21 June 2019	Ascending	18	27 June 2020	Ascending
7	27 July 2019	Ascending	19	21 July 2020	Ascending
8	20 August 2019	Ascending	20	16 August 2020	Ascending
9	25 September 2019	Ascending	21	19 September 2020	Ascending
10	31 October 2019	Ascending	22	25 October 2020	Ascending
11	24 November 2019	Ascending	23	30 November 2020	Ascending
12	30 December 2019	Ascending	24	24 December 2020	Ascending

Sentinel-1 SAR data were processed using the Sentinel Application Platform (SNAP). Each extracted satellite image was primarily subjected to a series of standard corrections to reduce error propagation in succeeding processes. Then, a time series analysis of the Sentinel-1 SAR data at VV and VH polarization was generated to analyze the variation of backscatter intensity of surfaces as a function of their vegetation characteristics.

3.2. Sentinel-2 Optical Data

Sentinel-2 was launched on 23 June 2015, focusing on providing visual information that can be applied to agriculture, land ecosystems monitoring, forest management, inland and coastal water quality monitoring, disaster mapping, and civil security. The satellite allows a 290 km field of view to collect a $100 \times 100 \text{ km}^2$ tile with various spatial resolutions, ranging from 10 m, 20 m, and 60 m.

Sentinel-2 optical data were obtained from ESA's Copernicus Open Access Hub. The data obtained were between 1 January 2019 and 31 December 2020 (Table 2). Once data had been retrieved, the files were extracted to obtain the spectral bands, clipped to the chosen location for the cropland and grassland areas. These optical data were obtained in Level 1C (L1C) and Level 2A (L2A). L1C is obtained from the top-of-atmosphere reflectance, which still includes the atmospheric cover, which requires dark object subtract 1 (DOS1) atmospheric correction from QGIS and other sentinel-based applications. L2A is obtained

from the bottom-of-atmosphere, which automatically removes the atmospheric cover, allowing for more immediate and accurate results without any correction.

Table 2. Sentinel-2 optical data used in the study.

No.	Acquisition Date	No.	Acquisition Date	No.	Acquisition Date
1	31 January 2019	9	13 September 2019	17	5 May 2020
2	25 February 2019	10	28 October 2019	18	29 June 2020
3	27 March 2019	11	22 November 2019	19	19 July 2020
4	26 April 2019	12	22 December 2019	20	18 August 2020
5	1 May 2019	13	31 January 2020	21	17 September 2020
6	20 June 2019	14	20 February 2020	22	2 October 2020
7	5 July 2019	15	21 March 2020	23	21 November 2020
8	29 August 2019	16	20 April 2020	24	11 December 2020

Sentinel-2 optical data were processed using the quantum geographic information system (QGIS) software, an open-source, cross-platform application. If the data is obtained in L1C, the whole file is placed into the DOS1 atmospheric correction procedure before applying it to the raster calculator function, which estimates the NDVI value per pixel, generating an NDVI map.

3.3. SPI Calculation

Meteorological data from three automatic weather stations in the Ilocos Norte Region from 2018 to 2020 were obtained. The data included daily precipitation, monthly precipitation, and daily average temperature. All meteorological observation data were acquired through PAGASA.

The calculation of the SPI was achieved through the use of Microsoft Excel software, where the precipitation data were programmed to the formula developed by [58]. As such, it was computed using Equations (1) and (2):

$$SPI = (P_i - P) / S \tag{1}$$

$$S = \sqrt{\sum (P_i - P)^2 / n} \tag{2}$$

where P_i is the rainfall of the given period, S is the standard deviation, P is the average of the period of the rainfall, and n is the number of data in a single period.

This study used a 1-month time scale to present precipitation anomalies and detect dryness or wetness in 2019 and 2020. This time scale reflected moisture conditions and seasonal estimation of precipitation. Positive SPI values obtained from monthly rainfall denote more significant precipitation than median precipitation, whereas negative SPI values indicate less than medium precipitation. Specifically, it was further classified to account for drought-related rainfall deviations (Table 3).

Table 3. SPI categories.

Anomaly	Range of SPI Values	Precipitation Regimes
Positive	$2 < SPI \leq \text{Max}$	Extremely wet
	$1.5 < SPI \leq 2$	Very wet
	$1 < SPI \leq 1.5$	Moderately wet
None	$-1 < SPI \leq 1$	Normal precipitation
Negative	$-1.5 < SPI \leq -1$	Moderately dry
	$-2 < SPI \leq -1.5$	Very dry
	$\text{Min} < SPI \leq -2$	Extremely dry

3.4. KBDI Calculation

The measurements needed for this drought index were the 24-h precipitation, the daily maximum air temperature, and the long-term mean annual precipitation. All these data were obtained from the climatological division of PAGASA. Three years' worth of data (2018 to 2020) was requested from the PAGASA and was utilized in this study. The measurements from 2018 were only used to initialize the KBDI value to be used on the first day of 2019. The previous day's drought index was needed to calculate the current day's drought index. This index cannot simply be set to zero since a KBDI equal to zero would mean that the soil is saturated. Thus, this assumption cannot be made at any given time. Therefore, an initialization procedure was required. First, the week of maximum precipitation from the first year of data (2018) was determined. The KBDI for that week was set to zero. This week was established as the initial point and served as the basis for the next day's KBDI. At this point, the calculated KBDI values were considered stabilized, and the initialization was completed. The KBDI on the last day of 2018 was then used to calculate the KBDI on the first day of 2019, and so forth until the end of 2020.

3.5. Correlation Analysis

Data analysis of various drought-related parameters was conducted using multiple time series graphs, which involved the different indices and data used in this study to observe and present data patterns as months passed from 2019 to 2020. Time graphs were performed monthly to show trends and correlations between different indices.

3.5.1. Relationship between Sentinel-1 Backscatter Coefficient and Sentinel-2 NDVI

Pearson's correlation analysis was used to investigate the relationship between the backscattering coefficients of VV and VH polarization from Sentinel-1 SAR data and NDVI values from Sentinel-2 optical data for the dry and wet seasons. This statistical parameter was applied to measure the strength of the association of SAR data with NDVI to estimate vegetation variations. Equation (3) describes the relationship between the two remote sensing data:

$$y = b_0 + b_1x \quad (3)$$

where y is the backscattering intensity value, b_0 and b_1 are the coefficients of the linear regression modeling, and x is the NDVI value.

3.5.2. Relationship of Remotely Sensed Data with Meteorological Data

This study plotted a time series analysis using SAR and optical data for the dry and wet seasons. After this, the outcomes of such information for the cropland and grassland areas were correlated to various meteorological-based data (precipitation and temperature) to understand the relationship between different drought indicators. As such, the relationship and correlation between the following were determined—(a) SAR data and SPI, (b) SAR data and KBDI, (c) NDVI and SPI, (d) NDVI and KBDI, and (e) SPI and KBDI.

3.6. Drought Risk Management Plan

Six steps were considered in producing a drought risk management plan (Figure 2). Primarily, drought hazard was determined through previous events. These included any evidence of droughts in an area, such as the devastation of crops due to dry soil or lack of precipitation, allowing the most prone to drought risks to be identified. Next, the drought risks in an area were identified through different parameters and indices used in this study. Once these were known, drought forecasting was done, and an early warning system was formulated. Lastly, drought risk assessment and monitoring help provide recommendations and action plans to manage drought occurrences.



Figure 2. Drought risk management plan.

4. Results and Discussion

4.1. Comparison of VV and VH Channels

The study investigated the backscattering intensity values in VV and VH polarizations in the regions of interest of the study area for two years, as shown in Figure 3. As observed in Figure 3, the cross-polarized (VH) channel provides a lower backscatter value and more noticeable fluctuations than the co-polarized (VV) channel. Conversely, the signals of croplands in VV polarization were higher than the VH. These conditions exist due to VH channels having a more pronounced pattern for the vegetation conditions, which is known to be an effect of volume scattering [59]. Furthermore, a cross-polarized channel provides a lower backscattering value since only a proportion of polarized waves (vertical turning into horizontal) return as a signal to the sensor. A study on estimating winter crop fields and grasslands in France and Tunisia indicated that the VH radar backscattered signal is lower than the VV channel as it is more sensitive when characterizing vegetation cover [60]. Therefore, although the cross-polarized channel provides a lower backscatter signal than the co-polarized channel, the former provides better analysis and interpretation of land vegetation conditions.

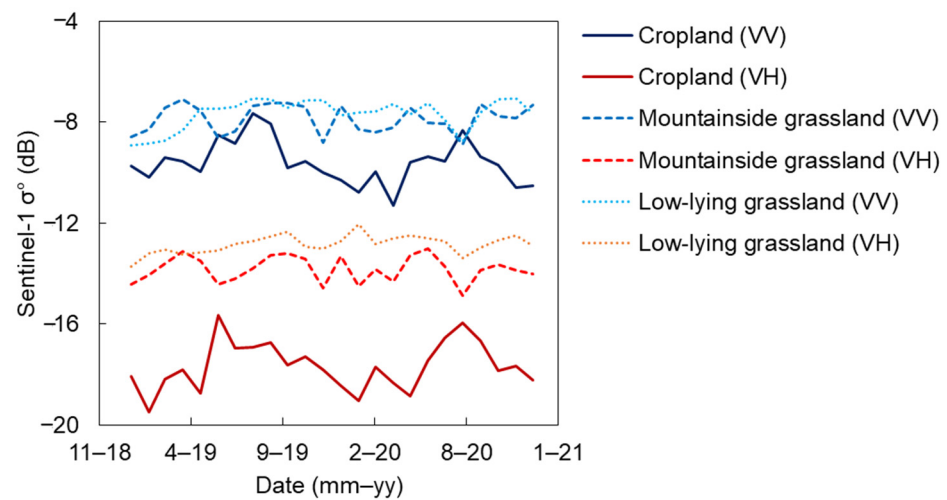


Figure 3. Time series of Sentinel-1 backscatter intensity coefficient (σ°) for the vertical-vertical (VV) and vertical-horizontal (VH) polarizations over cropland, mountainside grassland, and low-lying grassland in Ilocos Norte region, Philippines.

4.2. Temporal Analysis of Backscatter Intensity

4.2.1. Cropland Areas

Crop development is classified into three main phases: vegetative, reproductive, and maturation, as shown in Figure 4. First, the vegetative phase characterizes the crop’s initial development of tillers. Since this phase features the gradual increase in plant height, the backscattering signal σ° starts from a low value as the crop fields are initially dry. Several irregularities may be found in the vegetative phase in the backscatter intensity time series. Although there was a decrease in backscatter (from -16 dB to -17 dB in VH and -8 dB to -9 dB in VV) during the wet season, the intensity value at the end of the vegetative phase is still higher from its germination stage, indicating that the area is still experiencing a typical growth pattern. On the other hand, during the dry season, it is found that there is a general decrease in backscatter intensity (from -17 dB to -19 dB in VH and from -9 dB to -11 dB), which may show that rice crops are affected and do not conform with the conventional rice crop pattern.

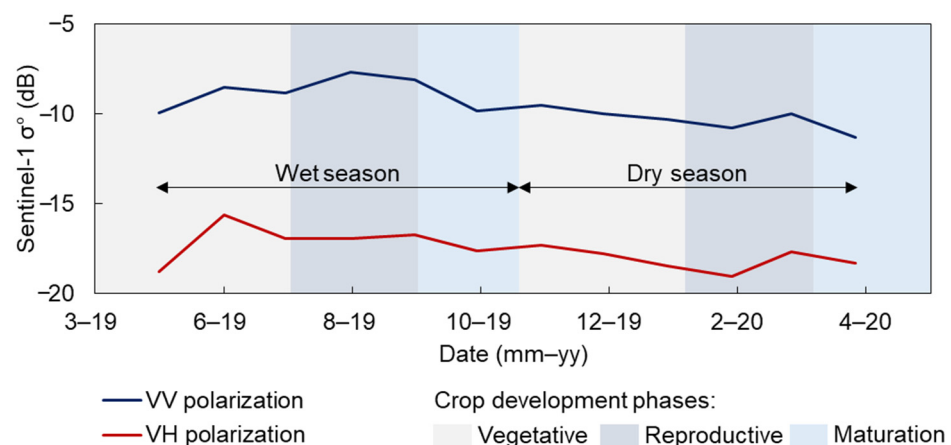


Figure 4. Time series of Sentinel-1 σ° for the vertical-vertical (VV) and vertical-horizontal (VH) polarizations over cropland areas in Ilocos Norte region, Philippines, indicating the three crop development phases—vegetative, reproductive, and maturation.

Secondly, the reproductive phase indicates that plant growth continues until it reaches its maximum height. From the start of this stage, the backscattering intensity decreases

as it approaches the end of the phase since the water content for crops is reduced upon completing the growing phase. However, a slight increase in the transmitted radar signal can be observed due to the vertical expansion of vegetation and, ultimately, an increase in the height and volume of rice crops. This pattern shows that the rise in the volume of vegetation causes an increase in the proportion of emitted signals. During the wet season, the backscatter intensity values for the reproductive phase characterize the typical rice crop growth as there was a decrease in radar signal from the start of this phase. It also revealed that a slight increase in backscatter intensity during August 2019 might be found, which indicates that this month is when the height of the rice crop is at its maximum.

On the other hand, an anomaly of the usual rice crop pattern is established during the dry season. A continuously decreasing trend shows that water content in the rice fields is lowered without the presence of a significant volume of vegetation. Furthermore, backscattering values for January to March 2020 are significantly lower than the vegetative phase (from -17 dB to -19 dB in VH and -9 dB to -11 dB in VV).

Lastly, the ripening or maturation phase is commonly identified with a continuous drying of leaves and stems. Unlike the previous crop growth stages, this phase reveals a constant decrease in σ° for both polarizations. From the study area, both the wet and dry seasons exhibited a decreasing backscattering intensity value. It must be noted that rice crops are normally harvested during the wet season, which indicates decreased vegetation volume and stems moisture content. On the other hand, during the dry season, radar signal in the maturation phase indicates low production during the harvesting period as the backscatter intensity at the end of the crop cycle (-18 in VH and -11 in VV) is lower compared to the end of the wet season (-17 dB in VH and -10 dB in VV).

4.2.2. Grassland Areas

Throughout the wet and dry seasons, both grassland areas exhibited a consistent medium to high backscatter coefficient, as shown in Figure 5. Radar signal for the mountainside grasslands ranges from -13 dB to -14 dB for VH and -7 dB to -8 dB for VV, whereas the low-lying grasslands were found at -12 dB to -13 dB for VH and -7 dB to -8 dB for VV. Since there are no significant fluctuations in radar signal throughout the entire time series, the backscattering signal for the grasslands reveals that the said regions of interest provided an almost uniform vegetation condition over time.

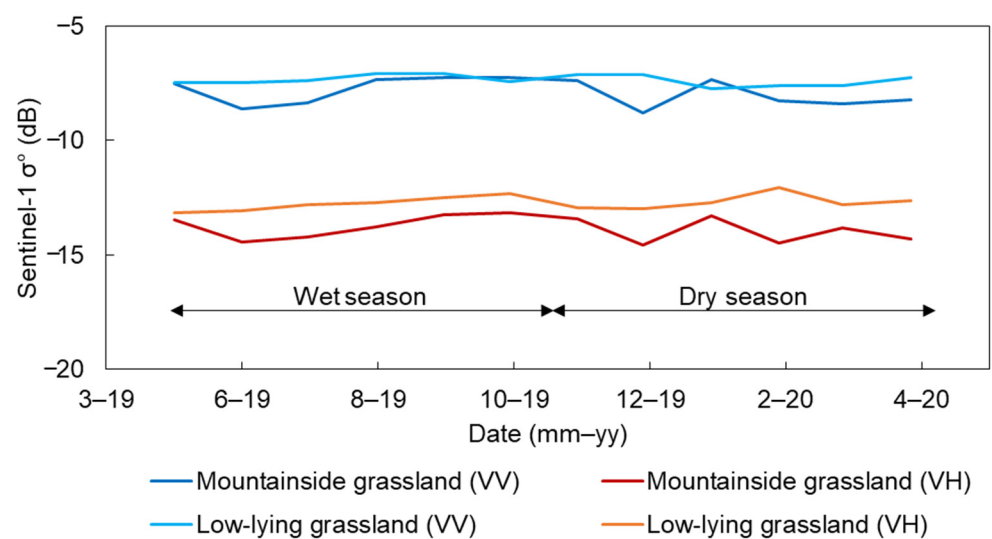


Figure 5. Time series of Sentinel-1 σ° for the vertical-vertical (VV) and vertical-horizontal (VH) polarizations over the mountainside grassland and low-lying grassland areas in Ilocos Norte region, Philippines.

Furthermore, since both grassland areas have low proximity to residential and agricultural loci, the regions of interest are barely affected, allowing less air pollution and creating an environment with improved air quality and unhindered soil nutrient content. Therefore, withstanding precipitation variabilities and being away from human intervention, the vegetation in the mountainside and low-lying grasslands does not exhibit significant drought risk throughout the two years.

4.3. Temporal Analysis of Sentinel-2 NDVI

In the analysis of NDVI, cropland areas varied significantly compared to both grassland areas. In the two years of analysis, its rise in value coincides with the start–peak–end period of rice planting in the Ilocos Norte region. As the area has also experienced differences in rainfall and temperature in the two years, despite the difference in value, the months where the NDVI has increased are still the same in both years, as shown in Figure 6. Cropland is easily more affected by factors in its surrounding, which may cause land degradation in an area, causing fewer values in its NDVI in a 10×10 m spatial resolution. In a single pixel, it cannot be avoided that other objects such as the soil, houses, water, and other objects surrounding the plants are included in a single pixel, which may cause a drop in NDVI value, leading to a need to be used with other drought indicators.

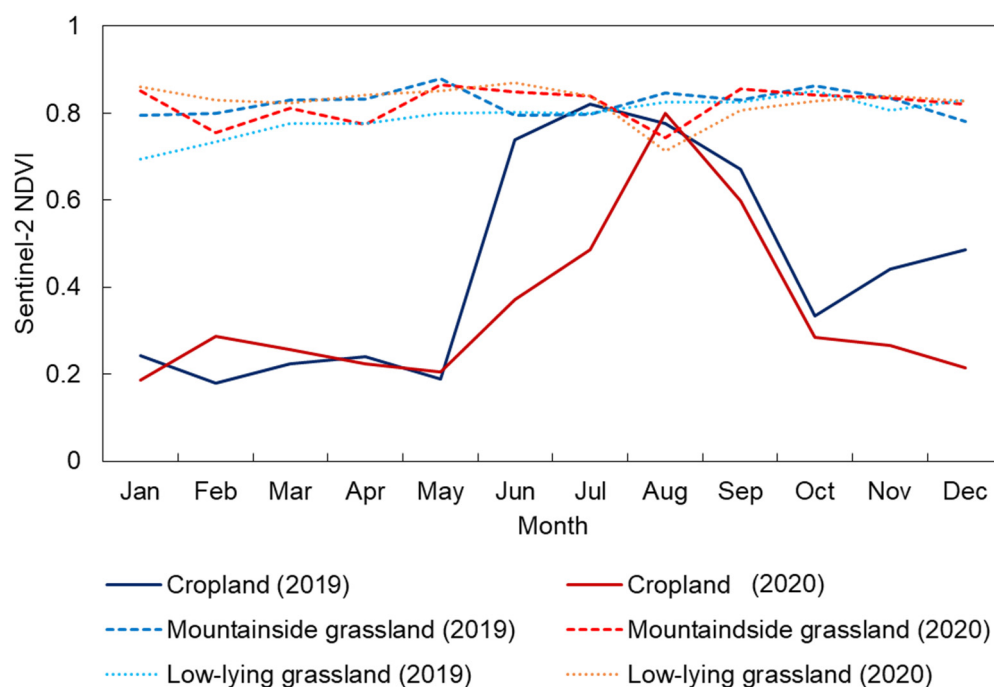


Figure 6. Monthly time series of Sentinel-2 normalized difference vegetation index (NDVI) over the cropland, mountainside grassland, and low-lying grassland areas in Ilocos Norte region, Philippines, for two years (2019 and 2020).

4.4. Temporal Analysis of SPI

Ilocos Norte has relatively average precipitation for the entire year (from 2019 to 2020) based on SPI, as shown in Figure 7. However, according to [58], drought is considered to be starting as SPI reaches a value of 0. The month of August peaked in the positive anomaly, followed by July for both years, which means that these were the months the location received the most amount of rainfall. Typhoons significantly impact these findings as, according to PAGASA, the peak typhoon season in the Philippines is from July to October. On the other hand, the months from October to June received minimal to no precipitation resulting in decreased soil moisture. These findings coincided with the reported drought events in the study location.

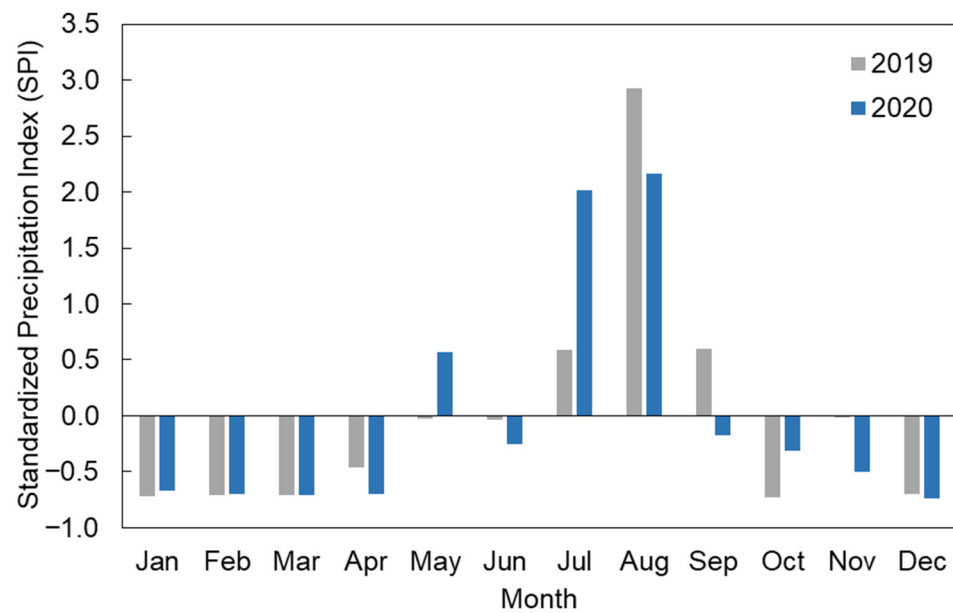


Figure 7. Standardized Precipitation Index (SPI) of the Ilocos Norte province in the Philippines for two years (2019 and 2020).

4.5. Temporal Analysis of KBDI

Results of the KBDI analysis show that the drought index is significantly high from December to May, which coincides with the province’s dry season, as shown in Figure 8. However, for June to November, the index trend is inconsistent, especially for the year 2020, where there was a noticeable spike in KBDI in June and from late July to early December. Natural phenomena can explain the erratic behavior of the drought index during the wet season, such as reported droughts and typhoons. Meanwhile, unlike the figure generated using the daily KBDI values, the trend of the average monthly KBDI is more consistent and aligns with the regular wet and dry seasons in Laoag City, which could explain the usual lapses in drought response in the region (Figure 9).

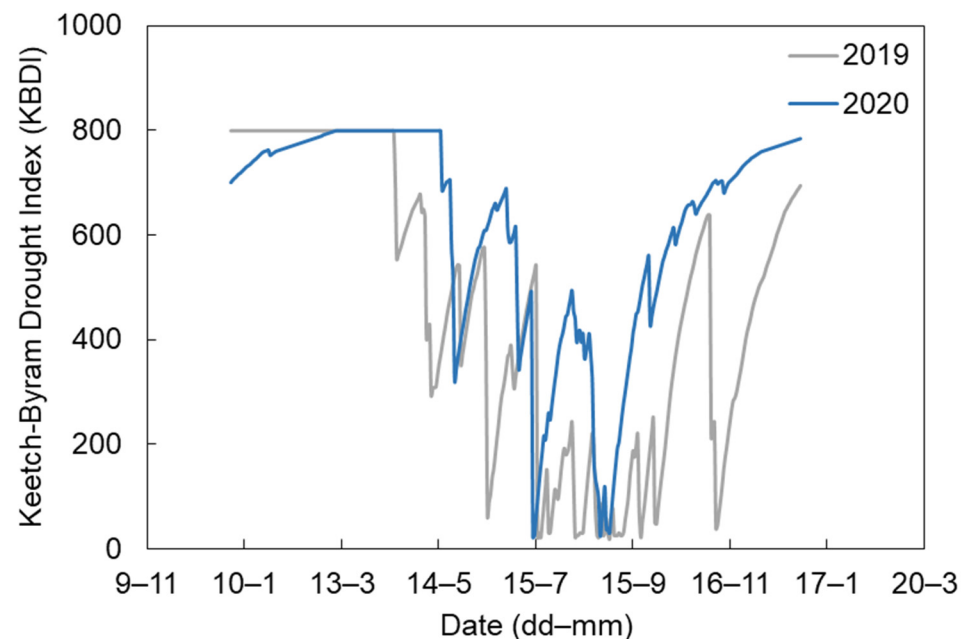


Figure 8. Daily Keetch-Byram drought index (KBDI) analysis results in Laoag City, Ilocos Norte province in the Philippines for 2019 and 2020.

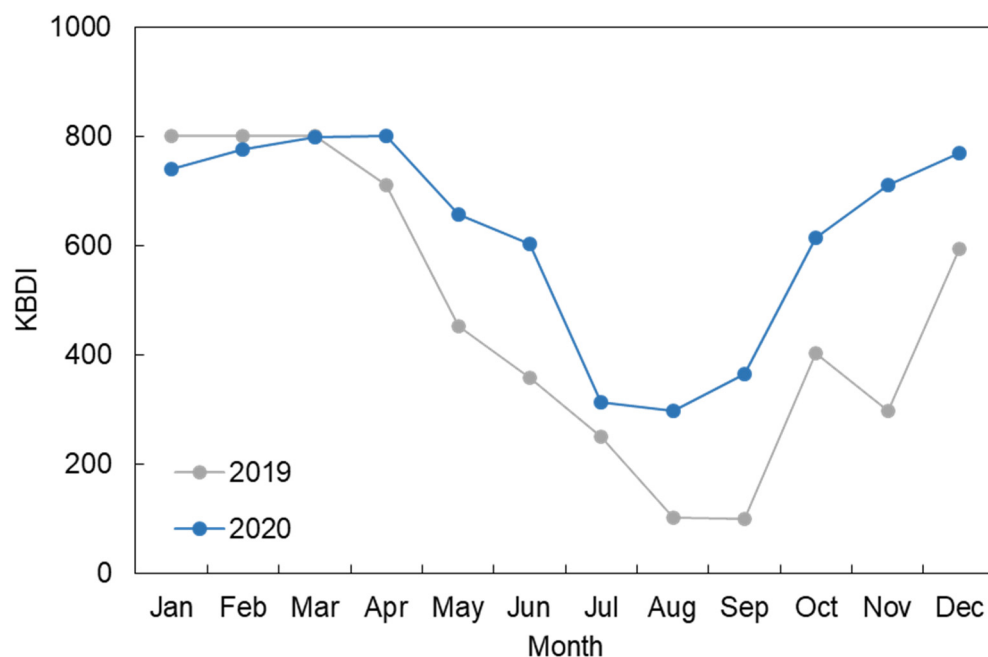


Figure 9. Average monthly KBDI analysis results in Laoag City, Ilocos Norte province in the Philippines for two years (2019 and 2020).

4.6. Correlation Analysis of Remote Sensing and Meteorological Drought Indicators

The study also investigated the potential of Sentinel-1 SAR data and Sentinel-2 optical data for drought monitoring, as shown in Figure A1 and Table 4. In investigating the potential of using remote sensing data for land monitoring and drought detection, the correlation analyses suggest that cross-polarized from backscattering coefficients appeared to be higher than co-polarized with NDVI. Consequently, it can be seen that the correlation results varied from 0.6 to 0.7. This statistical framework is also similar to the study of [61], which statistically quantified the relation between NDVI and backscatter intensity for sugarcane monitoring. The authors of [61] pointed out that the discrepancies from the perfect line fit can be traced to the slight difference in temporal resolution between the Sentinel-1 SAR data and Sentinel-2 optical data. It is known that the revisit time for Sentinel-1 and Sentinel-2 satellites is once every 12 and 10 days, respectively. Due to this, a comparison between the two remote sensing data would allow a slight difference in the observed scenarios and vegetation density for each pair of image acquisitions.

Table 4. Correlation results for SAR and optical data-derived drought indicators.

Area of Interest	R ²	
	VV Polarization	VH Polarization
Croplands	0.6414	0.7170
Mountainside grasslands	0.6123	0.7336
Low-lying grasslands	0.6224	0.6806

One of the objectives of this study is to determine if there is any significant correlation between remote sensing-based and meteorological-based drought indices, as summarized in Table 5. Various correlational analyses in this study reveal a generally low correlation between remote sensing data and meteorological-based data in grassland areas, as seen in the analysis between SPI and KBDI with the remote sensing-based indices backscatter intensity and NDVI. Meanwhile, a significant correlation could be observed between the data regarding croplands. The correlation difference is assumed to be caused by the varying slopes, elevations, and soil infiltration capacities in these two areas. Because

of some parameters, such as the type of crops and the distance between these crops or plants, it is assumed that croplands allow water to infiltrate the soil faster than grasslands. Precipitation in mountainside grasslands most likely ends up as runoff as well. Hence, the on-site condition in grasslands reflected by the satellite, which is used for remote sensing, cannot be accurately represented by meteorological data such as temperature and precipitation. The distance of ground equipment such as rain gauges and thermometers could be a factor as to why there is a correlation difference. The chosen cropland area for this study is closer to the automatic weather stations of PAGASA compared to the chosen grasslands. Despite this, it can still be concluded that there is an inverse relationship between KBDI and the remote sensing-based indices since an increase in KBDI signifies the occurrence of drought while a decrease in backscatter intensity and NDVI indicates less water on the surface and worsening of vegetation health, respectively.

Table 5. Summary of correlation results for remote sensing data and meteorological-based drought indices.

Drought Indices Correlation	Area of Interest	R ²	
		VV	VH
Backscatter intensity vs. SPI	Croplands	0.5160	0.3162
	Mountainside grasslands	0.0006	0.0006
	Low-lying grasslands	0.0024	0.0004
Backscatter intensity vs. KBDI	Croplands	0.6301	0.5600
	Mountainside grasslands	0.0012	0.0025
	Low-lying grasslands	0.305	0.0105
SPI vs. NDVI	Croplands		0.4701
	Mountainside grasslands		0.0006
	Low-lying grasslands		0.0053
KBDI vs. NDVI	Croplands		0.7066
	Mountainside grasslands		0.0105
	Low-lying grasslands		0.0035
SPI vs. KBDI	-		0.5542

4.7. Proposed EWS for Drought Risk Management

An EWS for drought occurrence is proposed in this study, seeing the significant results obtained from the four drought indices used in this study, as shown in Figure 10. This proactive mechanism allows stakeholders to utilize evidence-based and statistical decisions for drought assessment. Having been able to adapt the categories based on the National Drought Plan of the Philippines, the drought indices used in this study were provided with their corresponding threshold values that can assess monitoring, forecasting, and coping with the impacts of drought based on vegetation conditions and climatic characteristics.

Based on the specified threshold values from the study's drought indicators, the EWS is divided into four classifications to detect climate variabilities and identify vegetation and surface conditions. The first two decision ruling criteria are based on meteorological deficiency classified from SPI and KBDI. Since meteorological drought is the primary factor that affects crop growth, these parameters have been the first to be assessed. In this manner, the lack of rainfall and extreme temperatures may be a factor in drought risk. Consequently, the third and fourth assessments were based on the backscatter intensity and NDVI, which characterized the actual surface and vegetation conditions and provided better drought identification concerning crop vegetation health.

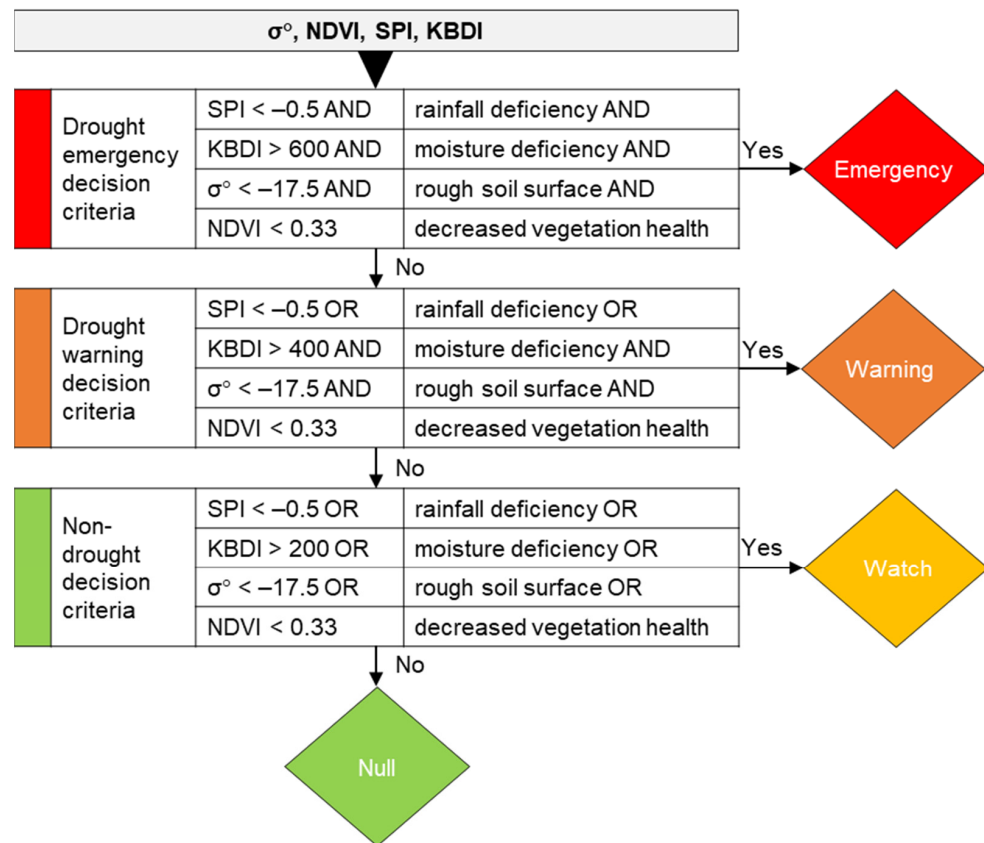


Figure 10. Proposed drought early warning system (EWS).

4.8. Implications

Drought is a natural phenomenon in the Philippines, especially in the Ilocos Norte region, where water shortage, warmer temperatures, and intensifying El Niño conditions negatively impact crop production. Meanwhile, RS and GIS are emerging data processing platforms with minimal applications in Southeast Asian countries. Considering this, the main objective of this study was to investigate the potential of RS and meteorological data in identifying the drought hazards in the cropland and grassland areas in Ilocos Norte. It also establishes the relationships between satellite SAR, optical, and meteorological-based drought indices, such as SPI and KBDI, for better drought risk assessment and crop monitoring.

This study analyzed the co-polarized (VV) and cross-polarized (VH) channels for the croplands, mountainside grasslands, and low-lying grassland areas in the Ilocos Norte region. The Sentinel-1 SAR data backscatter intensity results reveal the VH channel produces a lower return signal for all areas of interest than the VV channel. However, the former provides more observable variations in backscatter values during the two-year analysis period. This result was obtained as the VH channel presents a lower proportion of polarized waves returning to the satellite than the VV channel. Furthermore, due to its sensitivity in detecting structural changes in plants brought by volume scattering, the cross-polarized channel imparts a more excellent interpretation for characterizing vegetation cover. Thereby, the results of this investigation revealed the potential of multi-temporal analysis of Sentinel-1 SAR data for monitoring changes in vegetation conditions in the areas of interest.

Sentinel-1 backscatter analysis of the croplands area revealed the phenological rice crop phases. For both the dry and wet seasons, rice crop growth irregularities in the vegetative and reproductive stages were observed because of lower water content which, in turn, provided less than the usual amount of healthy vegetation. On the other hand, Sentinel-1 backscatter intensity values for the mountainside and low-lying grassland areas have also

been investigated in this study for drought. It was shown that there are no significant fluctuations of the Sentinel-1 backscatter coefficients for both VH and VV polarizations. Radar signals also reflect a consistent medium to high backscatter coefficient, indicating an almost uniform vegetation condition over the two-year analysis period. Furthermore, the elevation difference between the two grassland areas did not account for radar signal variability as the regions of interest have almost similar backscattering intensity values. Hence, as human activities do not impede the areas, mountainside and low-lying grasslands did not exhibit profound drought risk during 2019 and 2020.

Sentinel-2 NDVI is also analyzed in croplands, mountainside grasslands, and low-lying grasslands. Sentinel-2 NDVI data can immediately reveal all locations of interest, but the satellite optical data requires little to no cloud cover. The analysis of NDVI values reveals that NDVI is greatly affected by activities in nearby locations, despite having good crop health in an area. If the site is near roads and unvegetated lands, NDVI can significantly decrease its value. This situation can cause NDVI to need more confidence when dealing with drought and increase its reliance on other drought indicators presented in the study. However, it can still impart important, valuable information for agricultural purposes, such as peak months and vegetation health. When compared to the crop planting periods, the index can show a significant relation to the calendar, which is beneficial for identifying crop health per month.

As it is known that there was a drought in the early months of 2019, the NDVI values are identical when compared to the values in 2020. This finding created a pattern that farmers can use to identify when best to prepare for lower crop yields due to various factors related to environmental and climatic variabilities. As NDVI values are greatly affected by human activities, natural occurrences, such as typhoons, increased temperature, and other uncontrollable circumstances, including drought, will also affect its values as NDVI relies on a per-pixel visual representation than a direct analysis of a location. Like Sentinel-1 backscatter intensity values, NDVI can be used at any elevation and location if an available satellite optical image can be obtained from the RS database. These various reasons allow NDVI to be used as an index for different agricultural uses with some limitations due to its capacity to be affected by external factors.

The relationship between the two RS data was provided in the study to show the potential of Sentinel-1 and Sentinel-2 data in monitoring vegetation conditions. Correlation between backscattering intensity, in both VH and VV polarization, and NDVI values reveals a good correlation for the croplands, mountainside grasslands, and low-lying grasslands. This statistical data analysis also shows that the correspondence of NDVI with VH polarization was higher than the VV polarization, as the former provides more pronounced radar signals for vegetation conditions [46]. Hence, an increase in backscattering value corresponds to a greater NDVI, and at the same time, both agree to monitor vegetation conditions.

The results of SPI on a 1-month scale show that drought was present in the study location for 2019 and 2020. There is no standard index set as a threshold indicator for drought. Instead, researchers can fix it if the SPI value is less than 0. With that, even if the calculated index fell under the normal precipitation category, the study's results indicate that consecutive months of negative SPI value means that drought in terms of deficit in soil moisture is already starting. However, SPI only accounts for precipitation deficiency. SPI was correlated to another meteorological index, KBDI, and RS indices derived from Sentinel-1 and Sentinel-2 data to analyze its accuracy in drought indication further. SPI had a fair correlation with other indices with $R^2 > 0.50$ for cropland areas. However, there was no correlation for the grassland areas. This result suggests that the reliability of SPI in monitoring drought from the study's location is only limited to cropland areas. Despite that, sites with more ground equipment for collecting precipitation data may lead to different findings as to the effectiveness of SPI in monitoring drought in grassland areas.

Moreover, the KBDI accurately represented the weather conditions in the regions of interest through this study. This observation can be explained by natural phenomena, such

as tropical cyclones and drought occurrences in the province of Ilocos Norte. A significant correlation exists between KBDI and other indices, specifically in croplands. However, the correlation is significantly low for mountainside and low-lying grasslands. Therefore, using KBDI to determine the condition of plants in these areas is not recommended. It would be better to rely on NDVI as it represents vegetation health. For better utilization of meteorological indices such as KBDI and SPI, it is recommended to install more ground equipment. Ilocos Norte currently has only three automatic weather stations, which needs to be improved for the whole province. Installing rain gauges and weather thermometers in farmlands is advisable for more accurate monitoring. These installations will increase the reliability of KBDI and SPI, thus creating a simple yet effective system to observe and detect possible drought occurrences in these areas.

5. Outlook

Some studies have investigated the potential of seasonal and climatic forecasting for drought assessment. Still, studies have yet to explore the integration of such probabilistic outputs with observational satellite RS and meteorological data. This study analyzed the Sentinel-1 SAR data VV and VH channels for the cropland, mountainside grassland, and low-lying grassland areas in the Ilocos Norte region in the Philippines. The Sentinel-1 backscatter intensity results reveal that the VH channel produces a lower return signal for all regions of interest than the VV channel. However, the Sentinel-1 backscattering coefficient from the VH channel provides a better correlation, with $R^2 > 0.60$, with the Sentinel-2 NDVI in all regions of interest. Moreover, the Sentinel-1 backscattering coefficient and Sentinel-2 NDVI showed substantial irregularities in cropland areas compared to grassland areas. These results indicate that croplands are more affected by drought than grassland areas. A significant correlation exists between RS- and meteorological-based drought indicators, specifically KBDI, with backscattering coefficient and NDVI. On the contrary, SPI and KBDI show a poor correlation with the backscattering coefficient and NDVI, specifically in grassland areas of the Ilocos Norte region.

Nevertheless, the study contributes to the general understanding of climate-induced variations in crop production by characterizing climatic and vegetation variability for the cropland and grassland areas. Through quantifying vegetation conditions and precipitation deficiencies, this study highlights the feasibility of crop condition monitoring on a broader scale of environmental conditions. Thus, the overall outcome of the study presents that drought risk can be assessed appropriately by applying both RS data and meteorological-based drought indicators, allowing for a more outstanding establishment of drought risk management plans and early warning systems.

Author Contributions: Conceptualization, C.A.A., J.M.G., M.N.M., M.B.M. and R.R.; methodology, C.A.A., J.M.G., M.N.M. and M.B.M.; formal analysis, C.A.A., J.M.G., M.N.M., M.B.M. and R.R.; data curation, C.A.A., J.M.G., M.N.M. and M.B.M.; writing—original draft preparation, C.A.A., J.M.G., M.N.M. and M.B.M.; writing—review and editing, R.R.; supervision, R.R.; project administration, R.R. All authors have read and agreed to the published version of the manuscript.

Funding: This research received no external funding.

Data Availability Statement: Not applicable.

Acknowledgments: The authors thank the European Space Agency (ESA) for supplying Sentinel-1 and Sentinel-2 data free of charge. The authors also thank the Philippine Atmospheric, Geophysical, and Astronomical Services Administration for providing meteorological data free of charge.

Conflicts of Interest: The authors declare no conflict of interest.

Appendix A

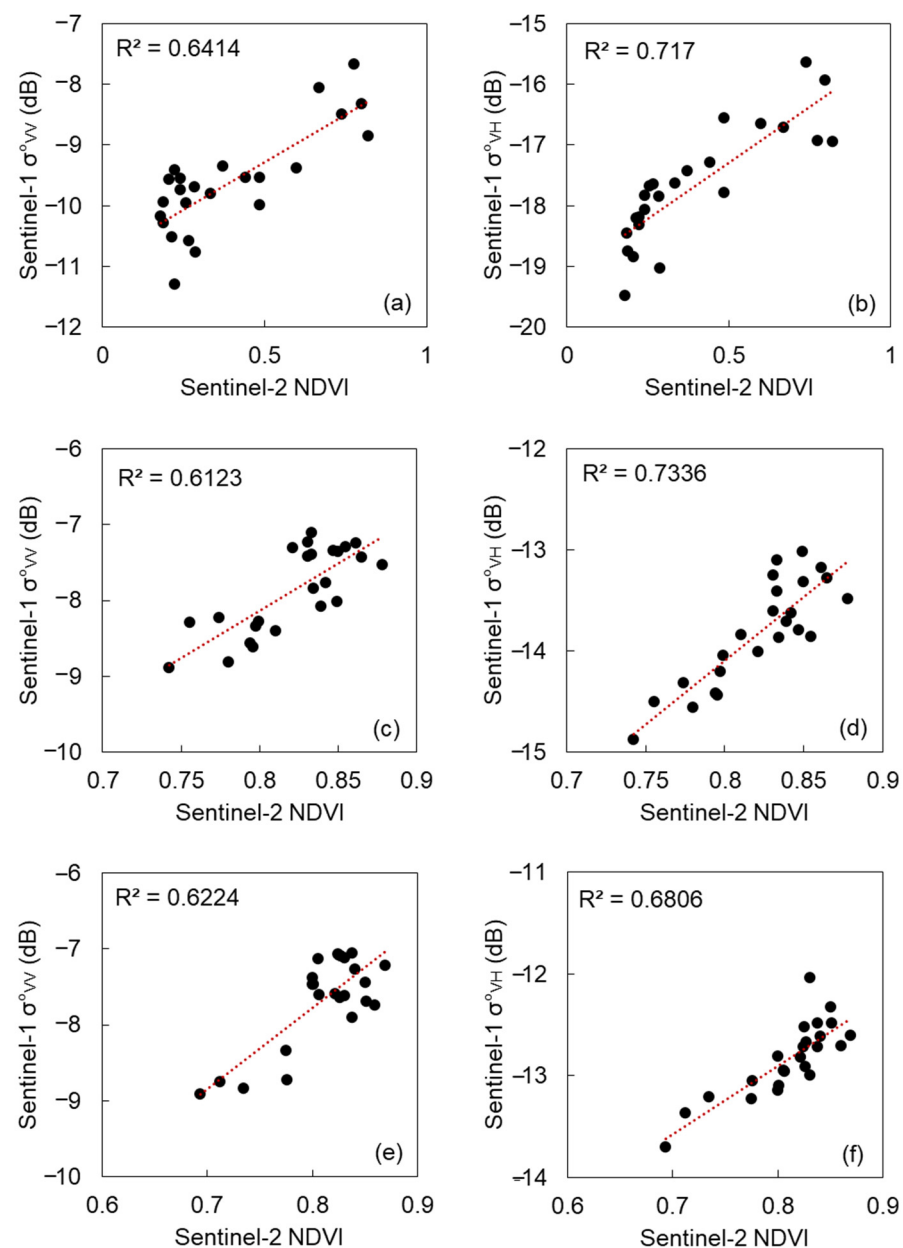


Figure A1. The relationship between Sentinel-1 σ^o (VV polarization) and Sentinel-2 NDVI over (a) cropland, (b) mountainside grassland, and (c) low-lying grassland areas. The relationship between Sentinel-1 σ^o (VH polarization) and Sentinel-2 NDVI over (d) cropland, (e) mountainside grassland, and (f) low-lying grassland areas.

References

1. Golian, S.; Mazdiyashi, O.; AghaKouchak, A. Trends in meteorological and agricultural droughts in Iran. *Theor. Appl. Clim.* **2015**, *119*, 679–688. [[CrossRef](#)]
2. Baudoin, M.A.; Vogel, C.; Nortje, K.; Naik, M. Living with drought in South Africa: Lessons learnt from the recent El Niño drought period. *Int. J. Disaster Risk Reduct.* **2017**, *23*, 128–137. [[CrossRef](#)]
3. Poornima, S.; Pushpalatha, M. Drought prediction based on SPI and SPEI with varying timescales using LSTM recurrent neural network. *Soft. Comput.* **2019**, *23*, 8399–8412. [[CrossRef](#)]
4. Bhunia, P.; Das, P.; Maiti, P. Meteorological drought study through SPI in three drought prone districts of West Bengal, India. *Earth Syst. Environ.* **2020**, *4*, 43–55. [[CrossRef](#)]

5. Fung, K.F.; Huang, Y.F.; Koo, C.H. Assessing drought conditions through temporal pattern, spatial characteristics and operational accuracy indicated by SPI and SPEI: Case analysis for Peninsular Malaysia. *Nat. Hazards* **2020**, *103*, 2071–2101. [[CrossRef](#)]
6. Pei, Z.; Fang, S.; Wang, L.; Yang, W. Comparative analysis of drought indicated by the SPI and SPEI at various timescales in inner Mongolia, China. *Water* **2020**, *12*, 1925. [[CrossRef](#)]
7. Liu, C.; Yang, C.; Yang, Q.; Wang, J. Spatiotemporal drought analysis by the standardized precipitation index (SPI) and standardized precipitation evapotranspiration index (SPEI) in Sichuan Province, China. *Sci. Rep.* **2021**, *11*, 1280. [[CrossRef](#)] [[PubMed](#)]
8. Ben, O.D.; Abida, H. Monitoring and mapping of drought in a semi-arid region: Case of the Merguellil watershed, central Tunisia. *Environ. Monit. Assess.* **2022**, *194*, 287.
9. Shaik, R.; NT, M. Estimation of annual regional drought index considering the joint effects of climate and water budget for Krishna River basin, India. *Environ. Monit. Assess.* **2020**, *192*, 472. [[CrossRef](#)]
10. Hu, Z.; Wu, Z.; Zhang, Y.; Li, Q.; Islam, A.; Pan, C. Risk assessment of drought disaster in summer maize cultivated areas of the Huang-Huai-Huai plain, eastern China. *Environ. Monit. Assess.* **2021**, *193*, 441. [[CrossRef](#)]
11. Bazrakshan, J.; Hejabi, S.; Rahimi, J. Drought monitoring using the multivariate standardized precipitation index (MSPI). *Water Resour. Manag.* **2014**, *28*, 1045–1060. [[CrossRef](#)]
12. Aghelpour, P.; Kisi, O.; Varshavian, V. Multivariate drought forecasting in short- and long-term horizons using MSPI and data-driven approaches. *J. Hydrol. Eng.* **2021**, *26*, 04021006. [[CrossRef](#)]
13. Ndlovu, M.S.; Demlie, M. Assessment of meteorological drought and wet conditions using two drought indices across KwaZulu-Natal Province, South Africa. *Atmosphere* **2020**, *11*, 623. [[CrossRef](#)]
14. Chahal, M.; Singh, O.; Bhardwaj, P.; Ganapuram, S. Exploring spatial and temporal drought over the semi-arid Sahibi river basin in Rajasthan, India. *Environ. Monit. Assess.* **2021**, *193*, 743. [[CrossRef](#)]
15. Dehghan, S.; Salehnia, N.; Sayari, N.; Bakhtiari, B. Prediction of meteorological drought in arid and semi-arid regions using PDSI and SDSM: A case study in Fars Province, Iran. *J. Arid. Land* **2020**, *12*, 318–330. [[CrossRef](#)]
16. Yang, Y.; Zhang, S.; Roderick, M.L.; McVicar, T.R.; Yang, D.; Liu, W.; Li, X. Comparing Palmer Drought Severity Index drought assessments using the traditional offline approach with direct climate model outputs. *Hydrol. Earth Syst. Sci.* **2020**, *24*, 2921–2930. [[CrossRef](#)]
17. Trenberth, K.E.; Dai, A.; van der Schier, G.; Jones, P.D.; Barichivich, J.; Briffa, K.R.; Sheffield, J. Global warming and changes in drought. *Nat. Clim. Chang.* **2014**, *4*, 17–22. [[CrossRef](#)]
18. Zhang, Q.; Shi, R.; Singh, V.P.; Xu, C.Y.; Yu, H.; Fan, K.; Wu, Z. Droughts across China: Drought factors, prediction and impacts. *Sci. Total Environ.* **2022**, *803*, 150018. [[CrossRef](#)] [[PubMed](#)]
19. Mishra, A.K.; Ines, A.V.M.; Das, N.N.; Khedun, C.P.; Singh, V.P.; Sivakumar, B.; Hansen, J.W. Anatomy of a local-scale drought: Application of assimilated remote sensing products, crop model, and statistical methods to an agricultural drought study. *J. Hydrol.* **2015**, *526*, 15–29. [[CrossRef](#)]
20. Zhang, X.; Chen, N.; Li, J.; Chen, Z.; Niyogi, D. Multi-sensor integrated framework and index for agricultural drought monitoring. *Remote Sens. Environ.* **2017**, *188*, 141–163. [[CrossRef](#)]
21. West, H.; Quinn, N.; Horswell, M. Remote sensing for drought monitoring & impact assessment: Progress, past challenges and future opportunities. *Remote Sens. Environ.* **2019**, *231*, 111291.
22. Xu, Z.; Cao, L.; Zhong, S.; Liu, G.; Yang, Y.; Zhu, S.; Luo, X.; Di, L. Trends in global vegetative drought from long-term satellite remote sensing data. *IEEE J. Sel. Top. Appl. Earth Obs. Remote Sens.* **2020**, *13*, 815–826. [[CrossRef](#)]
23. Javed, T.; Li, Y.; Rashid, S.; Li, F.; Hu, Q.; Feng, H.; Chen, X.; Ahmad, S.; Liu, F.; Pulatov, B. Performance and relationship of four different agricultural drought indices for drought monitoring in China's mainland using remote sensing data. *Sci. Total Environ.* **2021**, *759*, 143530. [[CrossRef](#)]
24. Shahzaman, M.; Zhu, W.; Ullah, I.; Mustafa, F.; Bilal, M.; Ishfaq, S.; Nisar, S.; Arshad, M.; Iqbal, R.; Aslam, R.W. Comparison of multi-year reanalysis, models, and satellite remote sensing products for agricultural drought monitoring over South Asian countries. *Remote Sens.* **2021**, *13*, 3294. [[CrossRef](#)]
25. Dotzler, S.; Hill, J.; Buddenbaum, H.; Stoffels, J. The potential of EnMAP and Sentinel-2 data for detecting drought stress phenomena in deciduous forest communities. *Remote Sens.* **2015**, *7*, 14227–14258. [[CrossRef](#)]
26. West, H.; Quinn, N.; Horswell, M.; White, P. Assessing vegetation response to soil moisture fluctuation under extreme drought using Sentinel-2. *Water* **2018**, *10*, 838. [[CrossRef](#)]
27. Hashim, B.M.; Sultan, M.A.; Attyia, M.N.; Al Maliki, A.A.; Al-Ansari, N. Change detection and impact of climate changes to Iraqi southern marshes using Landsat 2 MSS, Landsat 8 OLI and Sentinel 2 MSI data and GIS applications. *Appl. Sci.* **2019**, *9*, 2016. [[CrossRef](#)]
28. Puletti, N.; Mattioli, W.; Bussotti, F.; Pollastrini, M. Monitoring the effects of extreme drought events on forest health by Sentinel-2 imagery. *J. Appl. Remote Sens.* **2019**, *13*, 020501. [[CrossRef](#)]
29. Nguyen, M.D.; Baez-Villanueva, O.M.; Bui, D.D.; Nguyen, P.T.; Ribbe, L. Harmonization of Landsat and Sentinel-2 for crop monitoring in drought prone areas: Case studies of Ninh Thuan (Vietnam) and Bekaa (Lebanon). *Remote Sens.* **2020**, *12*, 281. [[CrossRef](#)]
30. Wieland, M.; Martinis, S. Large-scale surface water change observed by Sentinel-2 during the 2018 drought in Germany. *Int. J. Remote Sens.* **2020**, *41*, 4742–4756. [[CrossRef](#)]

31. Varghese, D.; Radulović, M.; Stojković, S.; Crnojević, V. Reviewing the potential of Sentinel-2 in assessing the drought. *Remote Sens.* **2021**, *13*, 3355. [[CrossRef](#)]
32. Benzougagh, B.; Meshram, S.G.; El Fellah, B.; Mastere, M.; Dridri, A.; Sadkaoui, D.; Mimich, K.; Khedler, K.M. Combined use of Sentinel-2 and Landsat-8 to monitor water surface area and evaluated drought risk severity using Google Earth Engine. *Earth Sci. Inform.* **2022**, *15*, 929–940. [[CrossRef](#)]
33. Kowalski, K.; Okujeni, A.; Brell, M.; Hostert, P. Quantifying drought effects in Central European grasslands through regression-based unmixing of intra-annual Sentinel-2 time series. *Remote Sens. Environ.* **2022**, *268*, 112781. [[CrossRef](#)]
34. Ngo, P.T.T.; Hoang, N.D.; Pradhan, B.; Nguyen, Q.K.; Tran, X.T.; Nguyen, Q.M.; Nguyen, V.N.; Samui, P.; Bui, D.T. A novel hybrid swarm optimized multilayer neural network for spatial prediction of flash floods in tropical areas using Sentinel-1 SAR imagery and geospatial data. *Sensors* **2018**, *18*, 3704. [[CrossRef](#)]
35. Landuyt, L.; Van Coillie, F.M.B.; Vogels, B.; Dewelde, J.; Verhoest, N.E.C. Towards operational flood monitoring in Flanders using Sentinel-1. *IEEE J. Sel. Top. Appl. Earth Obs. Remote Sens.* **2021**, *14*, 11004–11018. [[CrossRef](#)]
36. Harvey, M. Sentinel-1 InSAR captures 2019 catastrophic White Island eruption. *J. Volcanol. Geotherm. Res.* **2021**, *411*, 107124. [[CrossRef](#)]
37. Ramirez, R.A. The application of interferometric synthetic aperture radar (InSAR) on damage area mapping: The case of the 2020 Taal Volcano eruption. In Proceedings of the 2021 IEEE International Geoscience and Remote Sensing Symposium (IGARSS), Brussels, Belgium, 11–16 July 2021.
38. Qu, W.; Liu, B.; Zhang, Q.; Gao, Y.; Chen, H.; Wang, Q.; Hao, M. Sentinel-1 InSAR observations of co- and post-seismic deformation mechanisms of the 2016 Mw 5.9 Menyuan earthquake, Northwestern China. *Adv. Space Res.* **2021**, *68*, 1301–1317. [[CrossRef](#)]
39. Abcede, E.L.; Ajesta, A.; Alfonso, J.D.; Nucup, R.J.; Peralta, M.; Ramirez, R. InSAR-based detection and mapping of seismically induced ground surface displacement and damage in Pampanga, Philippines. *ASEAN Eng. J.* **2022**, *12*, 1–10. [[CrossRef](#)]
40. Dai, C.; Li, W.; Wang, D.; Lu, H.; Xu, Q.; Jian, J. Active landslide detection based on Sentinel-1 data and InSAR technology in Zhouqu County, Gansu Province, Northwest China. *J. Earth Sci.* **2021**, *32*, 1092–1103. [[CrossRef](#)]
41. Tzouvaras, M. Statistical time-series analysis of interferometric coherence from Sentinel-1 sensors for landslide detection and early warning. *Sensors* **2021**, *21*, 6799. [[CrossRef](#)] [[PubMed](#)]
42. Santangelo, M.; Cardinali, M.; Bucci, F.; Fiorucci, F.; Mondini, A.C. Exploring event landslide mapping using Sentinel-1 SAR backscatter products. *Geomorphology* **2022**, *397*, 108021. [[CrossRef](#)]
43. Cao, J.; Gong, H.; Chen, B.; Shi, M.; Zhou, C.; Lei, K.; Yu, H.; Sun, Y. Land subsidence in Beijing’s sub-administrative center and its relationship with urban expansion inferred from Sentinel-1/2 observations. *Can. J. Remote Sens.* **2021**, *47*, 802–817. [[CrossRef](#)]
44. Azarakhsh, Z.; Azadbakht, M.; Matkan, A. Estimation, modeling, and prediction of land subsidence using Sentinel-1 time series in Tehran-Shahriar plain: A machine learning-based investigation. *Remote Sens. Appl.-Soc. Environ.* **2022**, *25*, 100691. [[CrossRef](#)]
45. Espiritu, K.W.; Reyes, C.J.; Benitez, T.M.; Tokita, R.C.; Galvez, L.J.; Ramirez, R. Sentinel-1 interferometric synthetic aperture radar (InSAR) reveals continued ground deformation in and around Metro Manila, Philippines, associated with groundwater exploitation. *Nat. Hazards* **2022**, *114*, 3139–3161. [[CrossRef](#)]
46. Abdel-Hamid, A.; Dubovyk, O.; Graw, V.; Greve, K. Assessing the impact of drought stress on grasslands using multi-temporal SAR data of Sentinel-1: A case study in Eastern Cape, South Africa. *Eur. J. Remote Sens.* **2020**, *53*, 3–16. [[CrossRef](#)]
47. Maleki, S.; Rahdari, V.; Soffianain, A. Drought impact detection on wetlands in the arid area using synthetic aperture radar data. *Arab. J. Geosci.* **2022**, *15*, 919. [[CrossRef](#)]
48. Shorachi, M.; Kumar, V.; Steele-Dunne, S.C. Sentinel-1 SAR backscatter response to agricultural drought in The Netherlands. *Remote Sens.* **2022**, *14*, 2435. [[CrossRef](#)]
49. Urban, M.; Berger, C.; Mudau, T.E.; Heckel, K.; Truckenbrodt, J.; Odipo, V.O.; Smit, I.P.J.; Schmullius, C. Surface moisture and vegetation cover analysis for drought monitoring in the southern Kruger National Park using Sentinel-1, Sentinel-2, and Landsat-8. *Remote Sens.* **2018**, *10*, 1482. [[CrossRef](#)]
50. Ghazaryan, G.; Dubovyk, O.; Graw, V.; Kussul, N.; Schellberg, J. Local-scale agricultural drought monitoring with satellite-based multi-sensor time-series. *GISci Remote Sens.* **2020**, *57*, 704–718. [[CrossRef](#)]
51. Makineci, H.B. Seasonal drought analysis of Akşehir Lake with temporal combined sentinel data between 2017 and 2021 spring and autumn. *Environ. Monit. Assess.* **2022**, *194*, 529. [[CrossRef](#)] [[PubMed](#)]
52. International Disaster Database. Centre for Research on the Epidemiology of Disasters (CRED), Emergency Events Database (EM-DAT). Available online: <https://www.cred.be/> (accessed on 27 May 2022).
53. El Niño Wreaking Havoc in the Philippines. Asia Times. Available online: <https://asiatimes.com/2019/03/el-nino-wreaking-havoc-in-the-philippines/> (accessed on 27 May 2022).
54. Lucas, M.; Pabuayon, I. Risk perceptions, attitudes, and influential factors of rainfed lowland rice farmers in Ilocos Norte, Philippines. *Asian J. Agric. Dev.* **2011**, *8*, 61–78. [[CrossRef](#)]
55. Laborte, A.G.; Van Ittersum, M.K.; Van den Berg, M.M. Multi-scale analysis of agricultural development: A modeling approach for Ilocos Norte, Philippines. *Agric. Syst.* **2007**, *94*, 862–873. [[CrossRef](#)]
56. Galacgac, E.S.; Balicasan, C.M. Traditional weather forecasting for sustainable agroforestry practices in Ilocos Norte Province, Philippines. *Ecol. Manag.* **2009**, *257*, 2044–2053. [[CrossRef](#)]
57. Drought, Pests Hit Parts of Ilocos Norte. Philippine News Agency. Available online: <https://www.pna.gov.ph/articles/1116506> (accessed on 27 May 2022).

58. McKee, T.B.; Doesken, N.J.; Kleist, J. The relationship of drought frequency and duration to time scales. In Proceedings of the Eight Conference on Applied Climatology, Anaheim, CA, USA, 17–22 January 1993.
59. Vreugdenhil, M.; Navacchi, C.; Bauer-Marschallinger, B.; Hahn, S.; Steele-Dunne, S.; Pfeil, I.; Dorigo, W.; Wagner, W. Sentinel-1 cross ratio and vegetation optical depth: A comparison over Europe. *Remote Sens.* **2020**, *12*, 3404. [[CrossRef](#)]
60. Baghdadi, N.; El Hajj, M.; Zribi, M.; Bousbih, S. Calibration of the water cloud model at C-band for winter crop fields and grasslands. *Remote Sens.* **2017**, *9*, 969. [[CrossRef](#)]
61. Davidse, J. *The Relation between the NDVI and Backscatter of Sentinel-1 for Sugarcane Monitoring (Case Study in South Africa)*; Internship Report GRS-70424; Wageningen University: Wageningen, The Netherlands, 2015.

Disclaimer/Publisher’s Note: The statements, opinions and data contained in all publications are solely those of the individual author(s) and contributor(s) and not of MDPI and/or the editor(s). MDPI and/or the editor(s) disclaim responsibility for any injury to people or property resulting from any ideas, methods, instructions or products referred to in the content.